DC slice Imaging of CH3Cl photolysis at 193.3 nm

ARTICLE *in* THE JOURNAL OF PHYSICAL CHEMISTRY A · SEPTEMBER 2004

Impact Factor: 2.69 · DOI: 10.1021/jp0490756

3 AUTHORS, INCLUDING:

Suk Kyoung Lee
Wayne State University
23 PUBLICATIONS **448** CITATIONS

DC Slice Imaging of CH_3Cl Photolysis at 193.3 nm†

Dave Townsend,*,‡,§ Suk Kyoung Lee,‡,§ and Arthur G. Suits§,||

Department of Chemistry, SUNY Stony Brook, Stony Brook, New York 11794, Chemistry Department, Brookhaven National Laboratory, Upton, New York 11973, and Department of Chemistry, Wayne State University, Detroit, Michigan 48202

Received: March 1, 2004; In Final Form: May 13, 2004

The DC slice imaging method is used to record energy- and angle-resolved distributions for both ground-state Cl ($^2P_{3/2}$) and spin−orbit excited Cl* ($^2P_{1/2}$) photofragments produced from the Ã-band photolysis of CH_3Cl at 193.3 nm. The dissociation is found to be highly impulsive, with ∼90% of the available energy being released into translation. The angular distributions are predominantly perpendicular in the case of both the ground state and spin−orbit excited chlorine atom fragments, as characterized by recoil-energy averaged values of $\beta = -0.46$ and $\beta^* = -0.74$ respectively, although we find considerable variation in both channels as a function of CH_3 internal energy. In contradiction with previous measurements, we conclude that the transition to the $^1Q_1$ state dominates much of the Ã-band profile, and this has significant implications for the description of the dissociation dynamics. Our findings are rationalized in terms of similar measurements performed with other methyl halides and their H atom substituted analogues.

1. Introduction

Over the past 25 years considerable effort has been invested in developing a detailed understanding of the initial electronic excitation and subsequent inter-surface dynamics that play a role in the Ã-band photolysis of both CH_3I[1−14] and CH_3Br.[15−18] Many recent studies have also investigated the fluorinated and chlorinated analogues of the methyl group.[19−29] In all of these cases, single photon absorption leads to a broad and unstructured continuum band that exhibits two dominant photofragmentation pathways:

$$\begin{aligned} CX_3Y \xrightarrow{h\nu} CX_3 + Y(^2P_{3/2}) \\ CX_3 + Y^*(^2P_{1/2}) \end{aligned} \qquad (1)$$

As was first demonstrated by Mulliken,[30] for a system of the type CX_3Y, the lowest lying electronic transition arises from the promotion of a nonbonding lone pair electron on the Y atom to a σ^* orbital localized along the C−Y bond. In the presence of spin−orbit coupling, the excited state electronic configuration gives rise to three optically accessible potential surfaces that are traditionally denoted $^1Q_1$, $^3Q_0$, and $^3Q_1$ (which correspond to $^1\Pi_1$, $^3\Pi_0$, and $^3\Pi_1$ in conventional Hund's case a notation). All three excited state surfaces are repulsive and dissociate rapidly compared to the time scale of molecular rotation.[1,31] Transitions to the $^1Q_1$ and $^3Q_1$ states are perpendicular in nature and asymptotically correlate with the exclusive formation of ground-state Y ($^2P_{3/2}$) atoms. Excitation to the $^3Q_0$ state is of parallel character and correlates with spin−orbit excited atom products, Y* ($^2P_{1/2}$). This is summarized graphically in Figure 1. Along the C−Y dissociation coordinate, these states do not interact in the equilibrium C_{3v} geometry. However, distortion of the molecular frame lowers the overall symmetry to C_s and this can result in a strong coupling between the $^1Q_1$ and $^3Q_0$ states. This coupling gives rise to a conical intersection that may produce a significant intersystem crossing as the molecule falls apart. Since the crossing point does not lie in the Franck−Condon region, the atomic product branching ratio and the associated fragment angular distributions may be rationalized in terms of the oscillator strength carried by the transition to each of the three states $^1Q_1$, $^3Q_0$, and $^3Q_1$ at a given excitation wavelength and the probability that intersystem crossing subsequently occurs as the fragments separate.

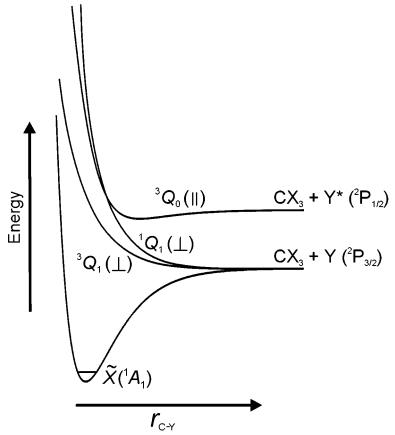

Figure 1. Schematic representation of the key elements that play a role in the Ã-band photolysis of the generic symmetric top molecule, CX_3Y, in the presence of significant spin−orbit coupling, along the C_{3v} reaction coordinate.

In the case of methyl iodide, the Ã-band absorption lies in the 210−350 nm region, with a maximum at ∼260 nm. Owing to the relative ease with which this range of wavelengths may be produced experimentally, CH_3I has been by far the most extensively studied of the methyl halide species. As first demonstrated by Gedanken and Rowe,[32] and later reaffirmed by subsequent investigations,[7,33] the parallel transition to the $^3Q_0$ surface is the overwhelmingly dominant absorption, with very weak perpendicular excitations directly to the $^1Q_1$ and $^3Q_1$

* Corresponding author. E-mail: David.Townsend@sunysb.edu.
† Part of the special issue "Richard Bersohn Memorial Issue".
‡ SUNY Stony Brook.
§ Brookhaven National Laboratory.
|| Wayne State University.

10.1021/jp0490756 CCC: $27.50
Published on Web 06/22/2004

surfaces only becoming significant at the extreme blue[4] and red wings[5−7] of the band, respectively. This observation is attributed to the large spin−orbit coupling induced by the presence of the iodine atom mixing the various excited states and bringing about an effective breakdown in the selection rules governing the restriction on singlet−triplet transitions (it is not known why the $^3Q_0$ transition is so much stronger than the $^3Q_1$ transition however). This behavior is reflected in the photofragment branching ratio, where [I*]/[I] > 3.0 across the majority of the absorption profile.[7,34] Additionally, the angular distribution of the dominant I* ($^2P_{1/2}$) channel exhibits a β-parameter which is very close to the limiting parallel value of 2.0. The observation of ground-state I ($^2P_{3/2}$) atoms is largely attributed to an intersystem crossing through the conical intersection formed between the $^1Q_1$ and $^3Q_0$ surfaces as the transition state distorts away from C_{3v} symmetry. This picture of predominantly indirect ground-state iodine atom formation is born out by the parallel character of the I ($^2P_{3/2}$) fragment angular distribution, with $\beta \sim 1.7$ at photolysis wavelengths shorter than ~300 nm.[7] This slightly reduced value of β relative to the near limiting behavior of β* observed in the spin−orbit excited iodine atom channel is a direct consequence of the distorted transition state geometry required to induce the inter-surface coupling. Far out on the red wing of the Ã-band absorption (λ > 300 nm), β ($^2P_{3/2}$) falls steadily to ~0.25 at 330 nm, and this effect may be attributed directly to increasing transition strength carried by the perpendicular transition to the $^3Q_1$ surface in this region. Additionally, the fraction of ground state iodine atoms produced rises considerably over this range, and although this observation may also be explained in part by the increased involvement of the $^3Q_1$ state (which correlates asymptotically with the formation of ground-state I atoms), it is known that the intersystem crossing transferring population from the $^3Q_0$ surface to the $^1Q_1$ surface also plays a key role since the possibility of this process occurring is significantly enhanced at longer wavelengths owing to the slower photofragment recoil velocity. It should be noted that the $^3Q_0$ and $^3Q_1$ surfaces are not thought to interact.[12,14]

The internal energy distribution of the methyl fragment following the dissociation of CH_3I has also been considered in many studies. It is generally accepted that the dissociation induces a degree of vibrational excitation within the CH_3 out-of-plane bending mode, ν_2, and that this is considerably more pronounced in the ground-state I ($^2P_{3/2}$) channel than in the I* ($^2P_{1/2}$) case, due to the different angles the C−H bonds make to the symmetry axis in the $^3Q_0$ and $^1Q_1$ states and the abrupt change in geometry that therefore occurs at the seam of the conical intersection.[12] Excitation of the CH_3 symmetric stretch, ν_1 (and more recently the asymmetric deformation, ν_4), has also been observed. Additionally, the end-over-end rotation (associated with the *N* quantum number) of the methyl fragments from the I ($^2P_{3/2}$) channel is found to be hotter than in the I* ($^2P_{1/2}$) channel, while the rotation about the principal symmetry axis (associated with the *K* quantum number) is cold in both instances. In the I ($^2P_{3/2}$) channel this is attributed to the zero-point vibration of the ν_6 bending mode in CH_3I inducing a "kick" to the departing CH_3 fragment at large separation distances (i.e., beyond the conical intersection) as the molecule falls apart. On the $^3Q_0$ surface (which correlates with the I* ($^2P_{1/2}$) channel) the steeper walls of the potential relative to $^1Q_1$ cause this motion to be suppressed. It should be noted that, although most studies investigating the internal state distributions of the CH_3 fragment agree qualitatively, the exact extent of both the rotational and vibrational energy partitioning has been the subject of some debate, a more thorough discussion of which may be found in the recent work of Eppink and Parker.[7,11]

Studies investigating the Ã-band absorption of CF_3I show very similar findings to those reported in CH_3I, with parallel absorption to the $^3Q_0$ surface again dominating over much of the absorption band and evidence of nonstatistical energy partitioning in the CF_3 fragment.[19−22,28,29] A subtle difference however is that the extent of the parallel character in the fragment recoil anisotropy of the I ($^2P_{3/2}$) channel is reduced relative to that in CH_3I, and this pathway is even observed to become predominantly perpendicular at excitation wavelengths >295 nm, indicating increased involvement of the low-lying $^3Q_1$ state.

The situation in methyl bromide is somewhat different from that encountered in methyl iodide. The Ã-band absorption is blue-shifted into the 175−270 nm region, with a maximum at around 202 nm.[35,36] Owing to the reduced spin−orbit interaction that results from replacing iodine with a lighter bromine atom, the restrictions governing singlet−triplet transitions become more strictly enforced. Electronic transitions to the $^3Q_0$ and $^3Q_1$ states are therefore now reduced in intensity relative to those to the $^1Q_1$ surface, and the cross sections for excitation to $^3Q_0$ and $^1Q_1$ in fact become comparable across much of the absorption band.[15,17] This change in relative transition strength is clearly observed in the bromine atom angular distributions, where the ground-state Br ($^2P_{3/2}$) fragments display predominantly perpendicular behavior across much of the absorption region. This is particularly pronounced on the blue wing of the band,[15,16] providing clear evidence for the greatly increased role of the $^1Q_1$ state compared to the situation in CH_3I. This change in the relative absorption strengths is also illustrated at longer wavelengths, where the anisotropy in both the Br ($^2P_{3/2}$) and Br* ($^2P_{1/2}$) channels is seen to fall considerably due to an increased propensity for intersystem surface crossing between dissociating species originating from both the $^3Q_0$ and $^1Q_1$ states. This is in contrast to the situation in CH_3I, where only the anisotropy in the I ($^2P_{3/2}$) channel is significantly reduced since the majority of the initial population is prepared exclusively on the $^3Q_0$ surface and significant transfer of population via the conical intersection can therefore only occur in one direction. As in CH_3I and CF_3I, there is also evidence of both vibrational (ν_2) and rotational excitation of the methyl fragment, particularly in the Br ($^2P_{3/2}$) channel.[17,18]

Limited studies investigating the Ã-band photolysis CF_3Br and CCl_3Br have also been carried out.[23−27] As in the case of CH_3Br, there is strong evidence for absorption to multiple surfaces in the initial excitation, in conjunction with significant intersystem crossings during the subsequent dissociation. One interesting point of note here is that, in the case of CCl_3Br photolysis at 234 nm, Jung et al.[26] report that both the Br ($^2P_{3/2}$) *and* Br* ($^2P_{1/2}$) channels display predominantly perpendicular anisotropy (as characterized by $\beta = -0.44$ and $\beta^* = -0.31$ respectively) and this represents the first example of such behavior in Ã-band dissociation studies of CX_3Y type species. This observation was attributed to a large (80%) contribution of the $^1Q_1$ surface to the total absorption in this instance, and although not directly addressed by the authors, one may speculate that the presence of the Cl atoms serves to reduce the overall extent of the spin-orbit coupling interaction.

The Ã-band absorption continuum of methyl chloride lies in the deep UV region between 165 and 230 nm. This system has been somewhat neglected in favor of the experimentally more convenient absorption bands of the bromide and iodide analogues, with very little information relating to the dissociation

dynamics having been reported. Kawasaki and co-workers first studied the photolysis of CH_3Cl at 193.3 nm using time-of-flight mass spectrometry and found the dissociation event to be well described by a simple impulsive model, with most of the available excess energy being released into fragment translation.[37] The [Cl*]/[Cl] branching ratio at 193.3 nm was first reported by Hirota and co-workers to be 0.50 ± 0.05, based upon time-resolved absorption profile measurements.[38] A subsequent investigation by Matsumi et al. employing Doppler spectroscopy determined the [Cl*]/[Cl] branching ratio to be 0.58 ± 0.05 and reported that the angular distribution for the ground-state Cl ($^2P_{3/2}$) atoms was almost exclusively of parallel character.[39,40] This observation was rationalized in terms of an initial excitation taking place to the $^3Q_0$ state—a parallel transition asymptotically correlated with the production of spin−orbit excited Cl* ($^2P_{1/2}$) atoms—with subsequent intersystem crossing to the $^1Q_1$ state giving rise to the appearance of the ground-state products. No measurement of the spin−orbit excited Cl ($^2P_{3/2}$) fragment angular distribution was reported in this study however. Similar findings were documented at the same photolysis wavelength by Dagdigian and co-workers, who quote a [Cl*]/[Cl] value of 0.62 ± 0.06 and who also observed a qualitatively parallel distribution for the Cl ($^2P_{3/2}$) fragments.[41] In addition, this study revealed the presence of a minor H atom elimination channel and demonstrated a profound change in the observed product state branching ratios and Cl ($^2P_{3/2}$) angular distribution when the fourth C−H overtone stretch of the methyl group was excited prior to interaction with the 193.3 nm beam. This was attributed to the vibrational excitation inducing a change in the nuclear dynamics of the same excited state potential surfaces as accessed in the case of internally cold CH_3-Cl, rather than the involvement of any additional electronic states. It should be noted at this point that the [Cl*]/[Cl] branching ratios of 0.58 ± 0.05 and 0.62 ± 0.06 that are quoted above were initially reported based upon $(2 + 1)$ REMPI line strength factors determined by Kawasaki and co-workers.[40] These values may be rescaled to 0.84 ± 0.07 and 0.89 ± 0.08, based upon subsequent studies of HCl dissociation by Wittig and co-workers.[42] A more recent paper by Ashfold and co-workers[43] confirms the observations of the Wittig group, and also provides a good review of this issue, to which the reader is directed for further information.

Further limited studies investigating the dissociation dynamics of ground-state CH_3Cl have been performed out on the extreme red edge of the $\tilde{A}$-band absorption at 212, 218, and 235 nm.[44,45] Importantly, at 212 and 218 nm there have been quantitative measurements of the Cl-atom angular distributions, and both the Cl ($^2P_{3/2}$) and Cl* ($^2P_{1/2}$) channels were found to be preferentially of parallel character, with each fragment channel exhibiting $\beta \sim 1.1$ at both wavelengths. As at 193.3 nm, the nature of the photofragment anisotropy was interpreted as the result of a dominant transition to the $^3Q_0$ surface.

The experimental findings reported to date in the case of CH_3-Cl are somewhat at odds with the original theoretical predictions of Mulliken,[30] who concluded that, in contrast to the case of CH_3Br and CH_3I, the weak spin−orbit interaction induced by the chlorine atom would bring about insufficient state mixing to produce any significant breakdown in the selection rules governing the restriction on singlet−triplet transitions. Absorption to the $^1Q_1$ surface should therefore be the dominant transition across almost all of the $\tilde{A}$-band in methyl chloride, and this assertion appears to be supported by the decomposition analysis of the band performed by Gedanken and Rowe using magnetic circular dichroism (MCD) spectroscopy.[32] Although the MCD work predates the small handful investigations into the dissociation dynamics described above, there have been no attempts to fully reconcile the discrepancies between these various studies or to quantify the dynamics to the same detailed extent as has been done previously with other methyl halide species. Here we present a new evaluation of the $\tilde{A}$-band absorption of methyl chloride at 193.3 nm based on data recorded using the recently reported DC slicing variant of the well-known photofragment imaging technique, as outlined in the following section.

2. Experiment

The key aspects of the experimental setup employed in the DC slice imaging approach have been described in detail elsewhere.[46] Only the points specific to this particular study will be summarized here. A molecular beam comprising 10% methyl chloride (stated purity 99.5%) seeded in argon was introduced into the source chamber of our differentially pumped apparatus at a backing pressure of ~2 bar. After passing through a skimmer, the collimated beam entered into a velocity mapping electrode assembly optimized for slice imaging and was then intersected at right angles by two counterpropagating laser beams. The photolysis laser (193.3 nm) was produced using an argon fluoride mini-excimer system (GAM EX10/600) running at 10 Hz. Polarization selection of the electric field vector was achieved by allowing this beam to pass through a "pile-of-plates" stack comprising a total of eight fused silica windows set at Brewster's angle. The electric field vector was chosen to be parallel to the imaging plane of the detector. The power of the photolysis laser was attenuated to approximately 400 μJ/pulse, and the beam was focused into the interaction region using a 30 cm lens. The probe laser was provided by frequency tripling the output of a dye laser (Continuum Jaguar, LDS 722 dye) pumped by the 532 nm harmonic of a Nd:YAG laser (Quanta Ray DCR-2). The polarization of this beam (~300 μJ/pulse) could be set either vertical or horizontal using a Soleil-Babinet compensator (Special Optics) before being focused through a second 30 cm lens. The Cl-atom photofragments produced in the dissociation event were initially probed using the following (2+1) REMPI schemes:

$$\mathrm{Cl}\ 3p^5(^2P_{3/2}) \xrightarrow{2h\nu} \mathrm{Cl}\ 3p^4 4p(^2D_{5/2}) \xrightarrow{h\nu} \mathrm{Cl}^+\ 236.284\ \mathrm{nm} \quad (2a)$$

$$\mathrm{Cl^*}\ 3p^5(^2P_{1/2}) \xrightarrow{2h\nu} \mathrm{Cl}\ 3p^4 4p(^2P_{3/2}) \xrightarrow{h\nu} \mathrm{Cl}^+\ 236.527\ \mathrm{nm} \quad (2b)$$

It should be noted however that several other nearby transitions were subsequently used as a means of confirming our experimental observations. The probe laser was calibrated with a wavemeter (Coherent WaveMaster), and the frequency of each resonant transition used was found to be in excellent agreement with previous work.[47] A second point of note here is that our initial interest in studying the dissociation of CH_3Cl at 193.3 nm stemmed from our ongoing investigations into the orbital polarization of atomic photofragments.[48,49] It was for this reason that majority of our data for the Cl ($^2P_{3/2}$) channel was collected utilizing the REMPI scheme proceeding via the $^2D_{5/2}$ state, as outlined above, rather than the more conventionally used Cl ($^2D_{3/2}$) ←← Cl ($^2P_{3/2}$) transition at 237.808 nm, since only the former case is expected to display any sensitivity to orbital alignment effects.[48,50]

Following ionization, chlorine ions are accelerated through the multilens velocity mapping assembly and impact upon a dual microchannel plate array of 120 mm diameter, which is coupled to a P-47 phosphor screen (Burle Electro-Optics). In

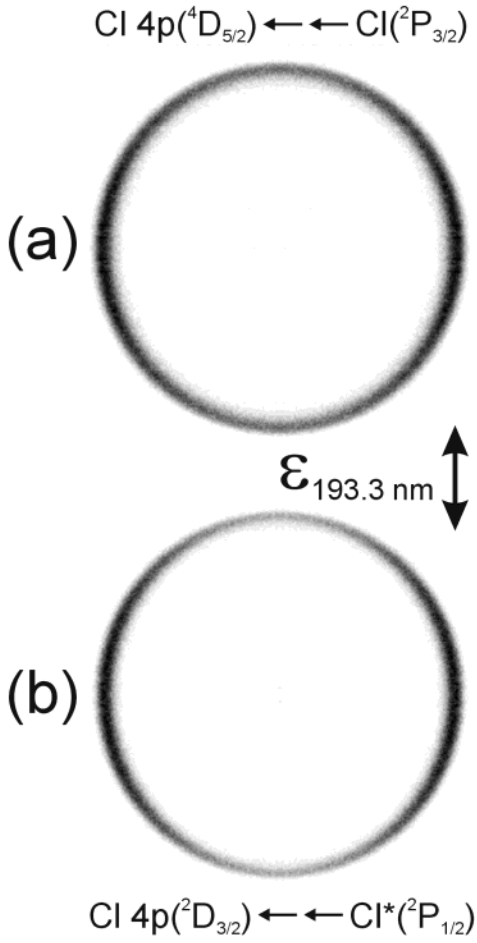

Figure 2. Images of (a) Cl ($^2P_{3/2}$) and (b) Cl* ($^2P_{1/2}$) from the 193.3 nm photodissociation of CH_3Cl, recorded using the (2 + 1) REMPI probe transitions as shown.

this particular instance a repeller electrode held at +850 V was used in conjunction with three additional focusing lenses in the velocity-mapping scheme to stretch the photofragment ion cloud along the time-of-flight axis to around 380 ns. The overall flight path from the laser interaction region to the detector was 105 cm. Application of a narrow (~50 ns) time gate at the detector was then sufficient to exclusively sample the central section of the distribution. A fully detailed description of this approach may be found in previous discussions.[46,49] The resulting image was recorded using a CCD camera (Mintron 2821e, 512 × 480 pixels) in conjunction with PC acquisition software (McLaren Research), which permitted real-time centroiding analysis of the data. The probe laser was repeatedly scanned across the Cl-atom Doppler profile during data acquisition. To ensure accurate velocity calibration of our apparatus, the image magnification factor of the ion lens assembly was determined by recording images of Cl ($^2P_{3/2}$) atoms produced during the 193.3 nm dissociation of HCl under identical experimental conditions. The scaling of our images was evaluated based upon the radius of the single sharp ring we observe experimentally in this case and that which would be expected purely on the basis of the chlorine atom time-of-flight and an accurate knowledge of the HCl bond energy.[51]

3. Results

Figure 2 shows the raw experimental sliced images recorded using the Cl ($^4D_{5/2}$) ← Cl ($^2P_{3/2}$) and Cl ($^2D_{3/2}$) ← Cl* ($^2P_{1/2}$) REMPI transitions, as described in the previous section. Other

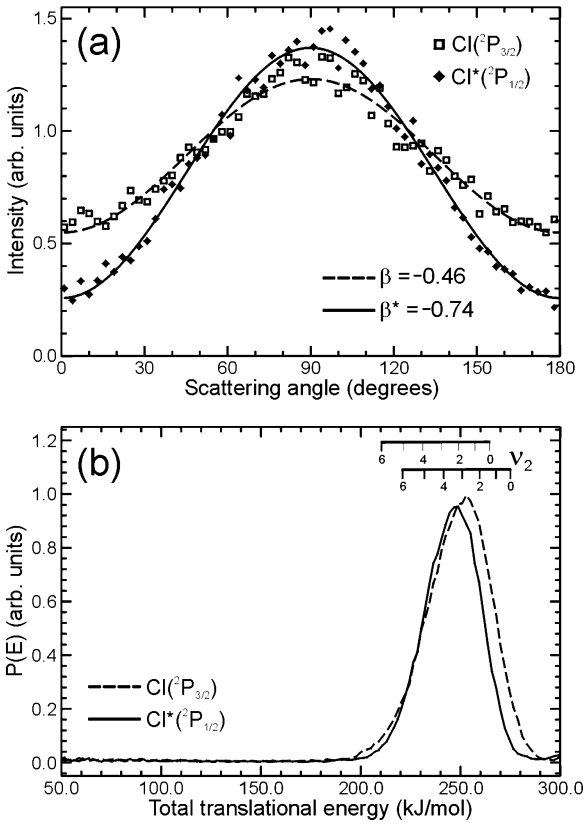

Figure 3. (a) Angular distributions of Cl ($^2P_{3/2}$) and Cl* ($^2P_{1/2}$) photofragments resulting from the 193.3 nm photolysis of CH_3Cl. (b) Translational energy release distributions for Cl ($^2P_{3/2}$) and Cl* ($^2P_{1/2}$). The peak areas have been scaled to reproduce a [Cl*]/[Cl] branching ratio of 0.86. The positions of the CH_3 ν_2 vibrational combs should only be regarded as a qualitative guide to the extent of any internal excitation, as discussed in the main text.

REMPI lines probing both ground and spin−orbit excited chlorine atoms gave rise to identical results. It is immediately apparent that the chlorine atom distributions exhibit significant spatial anisotropy and that this is predominantly perpendicular in character. Repeated switching of the probe laser polarization between 0 and 90° with respect to the photolysis beam produced no observable change in the spatial distribution or overall intensity of either image, indicating that the ground-state Cl ($^2P_{3/2}$) photofragments do not exhibit any significant orbital alignment. The recoil-energy averaged angular distributions for each fragmentation are plotted in Figure 3a along with the results obtained from fitting the data to the well-known β-parameter expression for the differential cross-section:

$$I(\theta) \propto 1 + \beta P_2(\cos\theta) \qquad (3)$$

The best-fit values of the velocity anisotropy parameters averaged over all photofragment recoil energies are $\beta = -0.46 \pm 0.03$ and $\beta^* = -0.74 \pm 0.03$ for the ground-state Cl ($^2P_{3/2}$) and spin−orbit excited Cl* ($^2P_{1/2}$) state chlorine atoms, respectively. The corresponding translational energy distributions (averaged over all recoil angles) are plotted in Figure 3b. The average kinetic energy release, $\langle E_T \rangle$, is calculated to be 252.8 ± 7.5 kJ/mol for the Cl channel and 248.6 ± 7.5 kJ/mol for the Cl* pathway. Note that the data in Figure 3b is scaled such that the ratio of the integrated area under the two peaks is 0.86—in order to meet agreement with previous measurements of the [Cl*]/[Cl] branching ratio, as discussed in section 1. The dissociation energy, D_0, of the C−Cl bond in methyl chloride has been recently determined to be 344.0 ± 0.4 kJ/mol.[52] At

the argon fluoride excimer photolysis wavelength, 193.3 ± 0.25 nm, the maximum energy available for release into fragment translation, E_{avl}, is therefore 275.0 ± 1.2 kJ/mol, and this calculated upper limit is in very good agreement with our experimental observations. The average fraction of the available energy released into translation, $f_T = \langle E_T \rangle / E_{avl}$, is 0.92 ± 0.03 in the case of Cl ($^2P_{3/2}$) production and, taking the magnitude of the spin−orbit splitting in chlorine to be 10.5 kJ/mol, it follows that $f_T = 0.94 \pm 0.03$ for Cl* ($^2P_{1/2}$) when only internal excitation of the methyl fragment is considered explicitly. These values are in reasonable agreement with the spin−orbit averaged measurement of $f_T = 0.85$ quoted by Kawasaki et al.,[37] and this value may be revised upward to 0.87 based upon the more accurate evaluation of D_0 that is now available.

Figure 3b also provides clear evidence for a difference in the internal energy distribution of the CH_3 fragments associated with the two dissociation pathways. This is illustrated in both the broader energy release distribution in the Cl ($^2P_{3/2}$) channel, and the fact that the difference in the value of f_T for the two channels is considerably smaller than the magnitude of the chlorine atom spin−orbit splitting. As discussed in section 1, based upon the outcome of previous investigations of CH_3I and CH_3Br photolysis, it would seem reasonable to assume that a large portion of this internal energy is partitioned within the CH_3 out-of-plane bending mode, ν_2. Overlaying the vibrational frequencies of Spirko and Bunker in Figure 3b,[53] it is clear that in both fragmentation channels there is a strong indication that several levels of ν_2 are populated, however, within the limits of our experimental resolution it is not possible to fully quantify this observation from this particular spectrum.

Examining Figure 2 in more detail it is apparent that in the case of the Cl* ($^2P_{1/2}$) channel, the distribution is considerably wider at 90° (horizontal) than at 0° (vertical), implying that the degree of CH_3 internal excitation is significantly less for fragments ejected parallel to the polarization vector of the photolysis laser than is the case for those ejected in a perpendicular direction. This angular variation in ring thickness is less pronounced in the Cl ($^2P_{3/2}$) channel. This observation is confirmed upon analyzing the angular dependence of the energy release distributions in more detail, as shown in Figure 4. In the Cl ($^2P_{3/2}$) channel the (scaled) distributions are very similar for two orthogonal recoil directions whereas for the Cl* ($^2P_{1/2}$) pathway the internal energy distribution of the CH_3 fragments is considerably narrower about the recoil direction parallel with the direction of photolysis laser polarization and peaks at a higher translational energy (i.e., lower internal excitation of CH_3) than is the case in the perpendicular direction.

In light of the recoil-angle dependence of the translational energy distribution, it is therefore unsurprising that both images in Figure 2 also exhibit a significant energy dependence in their respective angular distributions when analyzed more closely. This is shown in Figure 5, where both channels exhibit a steady decrease in β with increasing fragment translational energy. In the case of the Cl* ($^2P_{1/2}$) fragments, the slowest recoil speeds display a limiting perpendicular value of $\beta = -1$.

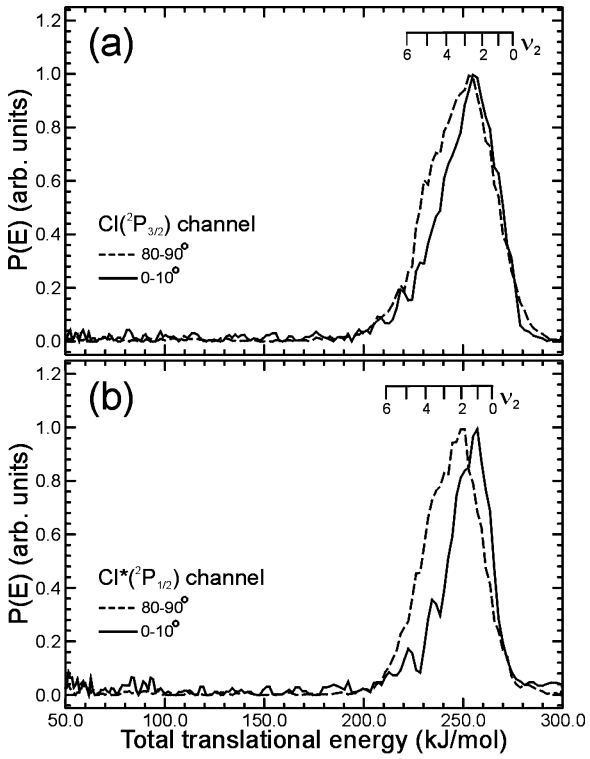

Figure 4. Normalized translational energy release distributions for photofragment ejection in two different angular regions following the 193.3 nm photolysis of CH_3Cl. (a) Cl ($^2P_{3/2}$) channel. (b) Cl* ($^2P_{1/2}$) channel. The positions of the CH_3 ν_2 vibrational combs should only be regarded as a qualitative guide to the extent of any internal excitation, as discussed in the main text.

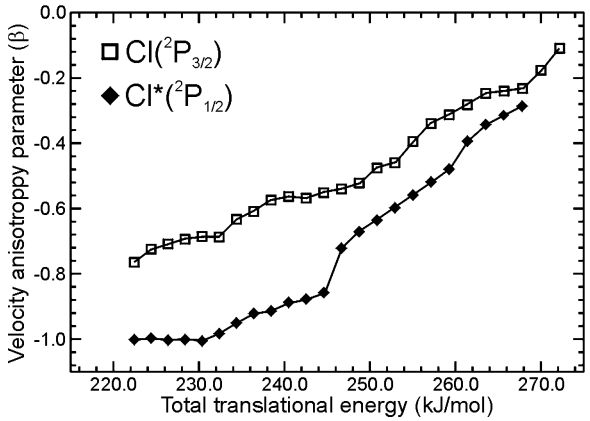

Figure 5. Velocity anisotropy parameter, β, vs photofragment translational energy for the Cl ($^2P_{3/2}$) and Cl* ($^2P_{1/2}$) channels following the 193.3 nm photolysis of CH_3Cl. Each β value has an associated error of ±0.05.

4. Discussion

The recoil-energy averaged anisotropy parameters of $\beta = -0.46 \pm 0.03$ and $\beta^* = -0.74 \pm 0.03$ that we obtain from our data demonstrate that both dissociation channels originate from predominantly perpendicular transitions. As outlined in section 1, and in contrast to previous results, this suggests excitation mainly to the $^1Q_1$ and/or $^3Q_1$ excited-state surfaces. However, the production of significant quantities of spin−orbit excited Cl* ($^2P_{1/2}$) photofragments and the considerable deviation of the anisotropy parameters from the limiting perpendicular value of −1.0 provides strong evidence for the involvement of the $^3Q_0$ surface and the influence of significant intersystem crossing on the dissociation dynamics.

For a pseudo-diatomic system such as CH_3Cl, along the C_{3v} coordinate the limiting case of a single surface dissociation occurring on a more rapid time scale than the period of molecular rotation would be expected to show values for β and β^* of −1.0 and +2.0, respectively—corresponding to either a purely perpendicular or purely parallel excitation. Additionally, the [Cl*]/[Cl] branching ratio observed under these conditions would therefore be directly correlated to the oscillator strength connecting the ground state to the various excited-state potential

surfaces. Deviations from this limiting case behavior may be a result of three distinct effects: (1) the influence of molecular rotation prior to dissociation, (2) distortion of the transition state, and (3) internal conversion and/or intersystem crossing between different fragment exit channels as the molecule falls apart. Following the approach first employed by Frey and Felder,[54] and used in several subsequent studies,[6,7,25−27] the relative contributions of these three processes to the overall dissociation dynamics may be determined directly from experimental measurements in the following manner.

For a given dissociation channel, the overall photofragment recoil anisotropy that is observed may be simply expressed as a weighted sum of the individual β-parameters arising from transitions to each excited state that can individually contribute to that channel in some way.

$$\beta_{\text{expt}} = \sum_i a_i \beta_i \tag{4}$$

In the specific case under consideration here, namely the Ã-band photolysis of methyl chloride at 193.3 nm, the above expression should therefore become a summation over transitions to the $^1Q_1$, $^3Q_1$, and $^3Q_0$ states. However, to significantly simplify our analysis, it is assumed that excitation to the $^3Q_1$ surface is negligible at this dissociation wavelength. This would seem to be a valid assertion since, as discussed in section 1, the only quantitative measurements of the Cl-atom angular distributions so far reported, at 212 and 218 nm,[44] exhibit preferentially parallel anisotropy. This suggests that out on the extreme red edge of the Ã-band absorption, excitation to the $^3Q_0$ surface starts to become dominant. Making the assumption that the energy ordering in the Franck−Condon region of the three allowed transitions that compose the Ã-band are the same as in methyl iodide—$^1Q_1 > {}^3Q_0 > {}^3Q_1$, as depicted in Figure 1—it is therefore reasonable to assume that the perpendicular character we observe at 193.3 nm comes from excitation to the $^1Q_1$ surface alone. Additionally, since there is strong evidence to suggest that the $^3Q_1$ surface is not coupled to either the $^1Q_1$ or $^3Q_0$ states,[12] its role in any intersystem crossing also need not be considered. The angular distributions for the Cl ($^2P_{3/2}$) and Cl* ($^2P_{1/2}$) fragments may therefore be defined as follows:

$$\beta_{\text{expt}}(\text{Cl}) = a_1\beta_{^3Q_0} + a_2\beta_{^1Q_1} \tag{5a}$$

$$\beta_{\text{expt}}(\text{Cl*}) = b_1\beta_{^3Q_0} + b_2\beta_{^1Q_1} \tag{5b}$$

where the expansion coefficients a_n and b_n are normalized such that

$$a_1 + a_2 = b_1 + b_2 = 1.0 \tag{5c}$$

At this point it should be noted that the above expressions assume that any interference effects resulting from the coherent excitation of multiple states leading to the same final product channel are negligible. It is well documented that such interference effects introduce additional modulations into the photofragment angular distribution that are sensitive to an adjustment of the probe laser polarization direction relative to the polarization used for the initial photolysis step.[48] Since in this case the angular distributions we observe are insensitive to any changes in this polarization geometry, this assumption appears to be confirmed in this case. The fraction of each pathway contributing to each final product state may therefore now be expressed in the following way:

TABLE 1: Recoil Energy Averaged Expansion Coefficients and Fractional Components Obtained for CH_3Cl Dissociation at 193.3 nm, As Described in the Main Text

a_1	a_2	b_1	b_2	$f^{^1Q_1}$	$f^{^1Q_1\rightarrow{}^3Q_0}$	$f^{^3Q_0}$	$f^{^3Q_0\rightarrow{}^1Q_1}$
0.18	0.82	0.09	0.91	0.44	0.43	0.04	0.09

$$f_{^3Q_0\rightarrow{}^1Q_1} = a_1\Phi_{\text{Cl}} \tag{6a}$$

$$f_{^1Q_1} = a_2\Phi_{\text{Cl}} \tag{6b}$$

$$f_{^3Q_0} = b_1\Phi_{\text{Cl*}} \tag{6c}$$

$$f_{^1Q_1\rightarrow{}^3Q_0} = b_2\Phi_{\text{Cl*}} \tag{6d}$$

where Φ is the photofragment quantum yield, as defined by

$$\Phi_{\text{Cl}} = \frac{1}{1 + \dfrac{[\text{Cl*}]}{[\text{Cl}]}} \tag{7a}$$

$$\Phi_{\text{Cl*}} = 1 - \Phi_{\text{Cl}} \tag{7b}$$

Parts a−d of eq 6 express the dynamics of the dissociation event in terms of its constituent parts, and one may therefore easily determine the relative transition strength for the initial excitation to each surface and then use this result to evaluate the intersystem crossing probability using

$$P_{^3Q_0\rightarrow{}^1Q_1} = \frac{f_{^3Q_0\rightarrow{}^1Q_1}}{f_{^3Q_0} + f_{^3Q_0\rightarrow{}^1Q_1}} \tag{8a}$$

$$P_{^1Q_1\rightarrow{}^3Q_0} = \frac{f_{^1Q_1\rightarrow{}^3Q_0}}{f_{^1Q_1} + f_{^1Q_1\rightarrow{}^3Q_0}} \tag{8b}$$

In the evaluation of eq 5, parts a and b, the anisotropy parameters $\beta^{^1Q_1}$ and $\beta^{^3Q_0}$ are assumed in this case to take values of −1.0 and 2.0, respectively (the limiting case values for instantaneous perpendicular and parallel dissociation). This is a clearly valid assertion in this instance since we observe values of $\beta = -1.0$ in our energy resolved angular distributions, as shown in Figure 5. From the work of Bersohn et al.,[1,55] we may deduce an upper state lifetime < 70 fs.

We first consider our recoil-energy averaged measurements. Table 1 summarizes the values which may be obtained from eqs 5a−c and 6a−d using a value of 0.86 for [Cl*]/[Cl], $\beta = -0.46$, and $\beta^* = -0.74$. As would be predicted qualitatively from the appearance of the experimental images in Figure 2, perpendicular excitation to the $^1Q_1$ state dominates the overall absorption at 193.3 nm, carrying 87% of the transition strength. There is however a nonnegligible (∼13%) contribution to the overall absorption that arises from direct parallel excitation to the $^3Q_0$ surface, indicating that spin−orbit mixing induced by the Cl-atom is still able lift the restriction on singlet−triplet transitions to some extent. In addition, there is significant transfer of population through the conical intersection formed between the $^1Q_1$ and $^3Q_0$ surfaces, as characterized by $P^{^3Q_0\rightarrow{}^1Q_1} = 0.69$ and $P^{^1Q_1\rightarrow{}^3Q_0} = 0.49$. Differences in the relative propensity for moving "up" and "down" through the conical intersection are not accounted for by simple diatomic models such as Landau−Zener theory, which invoke a one-dimensional "curve-crossing" picture of the interaction between different electronic states. Previous studies of CF_3Br and CCl_3Br have

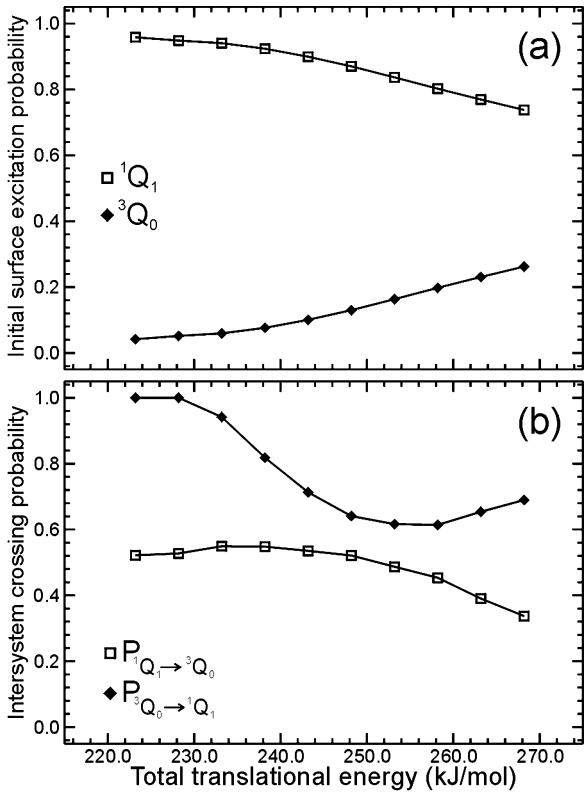

Figure 6. (a) Relative probability of intensity in a given photofragment channel originating from either the $^1Q_1$ or the $^3Q_0$ surface as a function of photofragment recoil energy. (b) Probability of the intensity appearing in a given photofragmentation channel via an intersystem crossing vs recoil energy.

reported observations similar to those presented here, however, quoting crossing probabilities which differ by more than a factor of 2 in some instances, and with $P^{3}_{Q_0 \rightarrow {}^1Q_1}$ always greater than $P^{1}_{Q_1 \rightarrow {}^3Q_0}$.[26,27] Analysis of the CH_3Br data of Kitsopoulos and co-workers[17] by the method outlined above also produces a similar picture. This variation in crossing behavior may be accounted for by the different geometries of the potential surfaces involved. In the case of CH_3I, theoretical studies have concluded that the $^1Q_1$ surface is steeper than in the $^3Q_0$ case along both the radial r(C−I) coordinate and also the off-axis distortion coordinate, ϕ.[12,14] Consequently, fragments dissociating on the $^1Q_1$ surface do so more rapidly and sample a smaller range of distorted geometries than in the $^3Q_0$ pathway, and the probability of an intersystem crossing taking place (which is dependent upon distortion away form the C_{3v} geometry) is therefore smaller in the former case. Although no such detailed theoretical studies have been reported for other analogous systems such as CH_3Br and CF_3Br, it is argued that the experimental observations relating to surface crossing behavior imply a similar situation must exist in these cases, and we also suggest that the same effect accounts for our findings in CH_3Cl.

The results of expanding our analysis to investigate the relative probability of intensity in a given photofragment channel originating from either the $^1Q_1$ or $^3Q_0$ surface as a function of photofragment recoil energy is presented in Figure 6a. The probability of the intensity appearing in a given channel via an intersystem crossing is shown relative to the recoil energy in Figure 6b. The required angular information is taken from Figure 5 and the relevant [Cl*]/[Cl] branching ratio may be estimated from the scaled data in Figure 3b. The key point of interest in Figure 6 is the sharp fall in the intersystem crossing probability from the $^3Q_0$ to the$^1Q_1$ surface with increasing photofragment recoil energy relative to the essentially constant value for $P^{1}_{Q_1 \rightarrow {}^3Q_0}$ across much of the distribution. It is difficult to account for this observation by simply invoking arguments relating to the shape of the relevant potential surfaces, and it would seem to suggest that the manner through which the internal energy is imparted into the dissociating molecule is different for initial excitation to the $^3Q_0$ and $^1Q_1$ states. As discussed in section 1, previous studies investigating both CH_3I and CH_3Br have shown that methyl fragments originating from the Cl ($^2P_{3/2}$) channel exhibit a considerable amount of vibrational excitation, particularly within the ν_2 bending mode, whereas the Cl* ($^2P_{1/2}$) pathway produces somewhat internally colder CH_3. This behavior may be attributed to a combination of two factors: (1) the geometry change upon initial excitation to the $\tilde{A}$-band, which is expected to be most significant (in the case of CH_3I) for the transition to the $^1Q_1$ state since the angle the C−H bonds make with the principal symmetry axis is 111.2, 103.9, and 90° in the ground, $^3Q_0$, and $^1Q_1$ states, respectively,[12] and (2) a sudden change in geometry at the seam of the conical intersection imparting additional energy into the out-of-plane bend as the molecule dissociates. In our CH_3Cl images, evidence for the same effects can clearly be observed, as illustrated in Figure 4—Cl* ($^2P_{1/2}$) fragments remaining exclusively on the $^3Q_0$ surface are directed primarily along 0° (vertical in Figure 2) and correlate with cold CH_3, whereas those fragments that initially populate the $^1Q_1$ state and then at some later time end up on $^3Q_0$ following intersystem crossing are preferentially ejected around 90° and produce internally excited methyl radicals (as a result of either mechanism 1 or 2). We note however that fully quantifying the internal energy distribution in the CH_3 fragments is impossible at this level of experimental resolution (±7.5 kJ/mol). The vibrational combs for the ν_2 mode in Figure 4 therefore merely serve as a qualitative guide to the overall extent of any internal excitation in the methyl radical.

In the ground-state Cl ($^2P_{3/2}$) channel, fragments originating from the $^3Q_0$ state that cross to $^1Q_1$ would appear to acquire a degree of internal excitation while passing through the conical intersection; hence, the distribution at 0° is wider than in the Cl* ($^2P_{1/2}$) channel. Fragments that traverse the $^1Q_1$ surface for the entire course of the dissociation still show a high amount of CH_3 internal excitation, however, implying that vibrational excitation imparted by the initial excitation is the most significant process in this instance. This picture is seemingly confirmed by Figure 6b, which demonstrates that fragments dissociating along the Cl* ($^2P_{1/2}$) pathway have an essentially constant probability of having got there via an intersystem crossing from the $^1Q_1$ surface, irrespective of the degree of internal CH_3 excitation, which would imply that a significant amount of the internal energy was imparted into the methyl chloride molecule prior to the region of the conical intersection. This is in contrast to excitation to the $^3Q_0$ state, where the molecule is vibrationally cold until passing through the conical intersection; hence, the probability of fragments appearing in the Cl ($^2P_{3/2}$) channel via an intersystem crossing from the $^3Q_0$ surface therefore seems elevated in the case of the slowest fragment recoil energies relative to those moving apart more rapidly. The slight divergence in the crossing probabilities at the fastest fragment energies in Figure 6b is most likely an artifact relating to the very small population in the Cl* ($^2P_{1/2}$) channel at this point and the large associated error in evaluating the photofragment quantum yields.

The central question raised by the results presented here is that of how well our findings fit in with existing measurements

reported for related systems and additionally, why our observations differ so dramatically with previous, albeit qualitative, observations of photofragment angular distributions resulting from methyl chloride photolysis at 193.3 nm. In the first case, our data would seem to conform to the original predictions of Mulliken, and MCD data of Gedanken and Rowe, in that the role of the $^3Q_0$ and $^3Q_1$ states in the Ã-band excitation of the methyl halides becomes less significant as the mass of the halogen atom decreases, due to weaker spin−orbit induced mixing with the $^1Q_1$ surface. Even on the red wing of the methyl chloride Ã-band, at 193.3 nm, our findings strongly suggest that $^1Q_1$ absorption is the principal transition and this leads us to conclude that this is the case across almost the entire absorption region. This is in contrast to the situation in CH_3Br where the comparable intensities of transitions to $^3Q_0$ and $^1Q_1$ play a key role in shaping the observed dynamics across much of the Ã-band, and in CH_3I where the $^3Q_0$ state is largely dominant, as discussed in more detail in section 1. Similar general trends are also directly observed in the analogous HX (X = F, Cl, Br, I) systems, the A-band absorptions of which have all been studied extensively.[42,43,57−60] Here, the absorption cross sections of the $^3\Pi(0)$ and $^3\Pi(1)$ states (which correspond to the $^3Q_0$ and $^3Q_1$ state labels in CH_3X) are known to rise progressively with the halogen atom mass due to increased spin−orbit mixing, as would be expected in CH_3X systems and as appears to be confirmed by our measurements.

The two previous reports of the Cl ($^2P_{3/2}$) photofragment angular distribution resulting from methyl chloride photolysis at 193.3 nm, as discussed in section 1, were based upon Doppler time-of-flight measurements.[39,41] In both cases, an *unpolarized* ArF excimer beam was used to initiate the dissociation step and we therefore speculate that this tended to obscure the true nature of the angular distribution in these earlier studies. Given the nonlimiting value of $\beta = -0.46$, we obtain for the Cl ($^2P_{3/2}$) fragments from our fully angle (and polarization) resolved measurements, this may be a plausible scenario.

One final point of note is the apparent absence of any significant orbital alignment in the Cl ($^2P_{3/2}$) fragments. As discussed previously, an interest in orbital polarization effects served as our initial motivation for investigating this system, and given the relatively large alignment previously observed in the 193.3 nm dissociation of HCl by Rakitzis et al.[61] (and also confirmed by our own experimental measurements[62]), the lack of any effect seems somewhat surprising. At 193.3 nm, the A-band absorption in HCl is almost exclusively (> 99%) via a perpendicular excitation to the $^1\Pi_1$ state,[42] although there is considerable intersystem crossing as the molecule falls apart, as indicated by the [Cl*]/[Cl] branching ratio of 0.69. Rakitzis et al. concluded that ~80% of the Cl ($^2P_{3/2}$) fragments populated $m_J = \pm^1/_2$ and that this arose predominantly from a coherent mechanism resulting from nonadiabatic transfer of population to the $^3\Pi_1$ state at very large fragment separation distances. This is in contrast the case of dissociation purely on the $^1\Pi_1$ state, where an incoherent alignment populating $m_J = \pm^3/_2$ exclusively is predicted.[61,63] Although the low-lying electronic states of CH_3-Cl are similar in character to those in HCl, we speculate that the significant absorption to the $^3Q_0$ surface (which is an order of magnitude larger than the corresponding transition to the $^3\Pi_0$ state in HCl) and high propensity for subsequent intersystem crossing to the $^1Q_1$ surface are sufficient to eliminate any incoherent alignment effects. Moving the photolysis wavelength to higher energies (where both the initial contribution of the $^3Q_0$ state and the probability of crossing to the $^1Q_1$ surface would be expected to be smaller) may permit the observation of incoherent polarization effects, however, although this has obvious practical difficulties. Additionally, coherent interactions at long range giving rise to coherent polarization may not take place in methyl chloride (or are too weak to give rise to an observable effect), possibly as a result of differing symmetry considerations.

Acknowledgment. The National Science Foundation supported this work under Award CHE-0102174. Acknowledgment is also made to the donors of the Petroleum Research Fund, administered by the American Chemical Society, for partial support of this research.

References and Notes

(1) Dzvonik, M.; Yang, S.; Bersohn, R. *J. Chem. Phys.* **1974**, *61*, 4408.
(2) van Veen, G. N. A.; Baller, T.; de Vries, A. E.; van Veen, N. J. A. *Chem. Phys.* **1984**, 405.
(3) Black, J. F.; Powis, I. *Chem. Phys.* **1988**, *125*, 375.
(4) Penn, S. M.; Hayden, C. C.; Muyskens, K. J. C.; Crim, F. F. *J. Chem. Phys.* **1988**, *89*, 2909.
(5) Fairbrother, D. H.; Briggman, K. A.; Weitz, E.; Stair, P. C. *J. Chem. Phys.* **1994**, *101*, 3787.
(6) Hertz, R. A.; Syage, J. A. *J. Chem. Phys.* **1994**, *100*, 9265.
(7) Eppink, A. T. J. B.; Parker, D. H. *J. Chem. Phys.* **1998**, *109*, 4758.
(8) Sparks, R. K.; Shobatake, K.; Carlson, L. R.; Lee, Y. T. *J. Chem. Phys.* **1981**, *75*, 3838.
(9) Barry, M. D.; Gorry, P. O. *Mol. Phys.* **1984**, *52*, 461.
(10) Loo, R. O.; Hall, G. E.; Haerri, H.-P.; Houston, P. L. *J. Phys. Chem.* **1988**, *92*, 5.
(11) Eppink, A. T. J. B.; Parker, D. H. *J. Chem. Phys.* **1999**, *110*, 832.
(12) Amatatsu, Y.; Morokuma, K.; Yabushita, S. *J. Chem. Phys.* **1991**, *94*, 4858.
(13) Person, M. D.; Kash, P. W.; Butler, L. J. *J. Chem. Phys.* **1990**, *94*, 2557.
(14) Amatatsu, Y.; Yabushita, S.; Morokuma, K. *J. Chem. Phys.* **1996**, *104*, 9783.
(15) van Veen, G. N. A.; Baller, T.; E., d. V. A. *Chem. Phys.* **1985**, *92*, 59.
(16) Hess, W. P.; Chandler, D. W.; Thoman, J. W., Jr. *Chem. Phys.* **1992**, *163*, 277.
(17) Gougousi, T.; Samartzis, P. C.; Kitsopoulos, T. N. *J. Chem. Phys.* **1998**, *108*, 5742.
(18) Underwood, J. G.; Powis, I. *Phys. Chem. Chem. Phys.* **2000**, *1*, 747.
(19) van Veen, G. N. A.; Baller, T.; de Vries, A. E.; Shapiro, M. *Chem. Phys.* **1985**, *93*, 277.
(20) Felder, P. *Chem. Phys.* **1990**, *143*, 141.
(21) Felder, P. *Chem. Phys.* **1991**, *155*, 435.
(22) Felder, P. *Chem. Phys. Lett.* **1992**, *197*, 425.
(23) Lee, Y. R.; Tzeng, W. B.; Yang, Y. J.; Lin, Y. Y.; Lin, S. M. *Chem. Phys. Lett.* **1994**, *222*, 141.
(24) Lee, Y. R.; Yang, Y. J.; Lin, Y. Y.; Lin, S. M. *J. Chem. Phys.* **1995**, *103*, 6966.
(25) Thelen, M. A.; Felder, P. *Chem. Phys.* **1996**, *204*, 135.
(26) Jung, Y.-J.; Park, M. S.; Kim, Y. S.; Jung, K.-H.; Volpp, H.-R. *J. Chem. Phys.* **1999**, *111*, 4005.
(27) Kim, T. K.; Park, M. S.; Lee, K. W.; Jung, K.-H. *J. Chem. Phys.* **2001**, *115*, 10745.
(28) Aguirre, F.; Pratt, S. T. *J. Chem. Phys.* **2003**, *118*, 1175.
(29) Furlan, A.; Gejo, T.; Huber, J. R. *J. Phys. Chem.* **1996**, *100*, 7956.
(30) Mulliken, R. S. *J. Chem. Phys.* **1940**, *8*, 382.
(31) Zhong, D.; Cheng, P. Y.; Zewail, A. H. *J. Chem. Phys.* **1996**, *105*, 7864.
(32) Gedanken, A.; Rowe, M. D. *Chem. Phys. Lett.* **1975**, *34*, 39.
(33) Johnson, B. R.; Kinsey, J. L. *J. Phys. Chem.* **1996**, *49*, 18937.
(34) Guo, H.; Schatz, G. C. *J. Chem. Phys.* **1990**, *93*, 393.
(35) Molina, L. T.; Molina, M. J.; Rowland, F. S. *J. Phys. Chem.* **1982**, *86*, 2672.
(36) Atkinson, R.; Baulch, D. L.; Cox, R. A.; Hampson, R. F., Jr.; Kerr, J. A.; Troe, J. *J. Phys. Chem. Ref. Data* **1992**, *21*, 1125.
(37) Kawasaki, M.; Kasatani, K.; Sato, H. *Chem. Phys.* **1984**, *88*, 135.
(38) Tiemann, E.; Kanamori, H.; Hirota, E. *J. Chem. Phys.* **1988**, *88*, 2457.
(39) Matsumi, Y.; Puspendu, K. D.; Kawasaki, M. *J. Chem. Phys.* **1990**, *92*, 1696.
(40) Matsumi, Y.; Das, P. K.; Kawasaki, M.; Tonokura, K.; Ibuki, T.; Inoue, G.; Satyapal, S.; Bersohn, R. *J. Chem. Phys.* **1992**, *97*, 5261.
(41) Melchior, A.; Lambert, H. M.; Dagdigian, P. J.; Bar, I.; Rosenwaks, S. *Isr. J. Chem.* **1997**, *37*, 455.

(42) Zhang, J.; Dulligan, M.; Wittig, C. *J. Chem. Phys.* **1997**, *107*, 1403.
(43) Regan, P. M.; Langford, S. R.; Ascenzi, D.; Cook, P. A.; Orr-Ewing, A. J.; Ashfold, M. N. R. *Phys. Chem. Chem. Phys.* **1999**, *1*, 3247.
(44) Lambert, H. M.; Dagdigian, P. J. *J. Chem. Phys.* **1998**, *109*, 7810.
(45) Lambert, H. M.; Dagdigian, P. J. *Chem. Phys. Lett.* **1997**, *275*, 499.
(46) Townsend, D.; Minitti, M. P.; Suits, A. G. *Rev. Sci. Instrum.* **2003**, *74*, 2530.
(47) Arepalli, S.; Presser, N.; Robie, D.; Gordon, R. J. *Chem. Phys. Lett.* **1985**, *118*, 88.
(48) Bracker, A. S.; Wouters, E. R.; Suits, A. G.; Vasyutinskii, O. S. *J. Chem. Phys.* **1999**, *110*, 6749.
(49) Townsend, D.; Lee, S. K.; Suits, A. G. *Chem. Phys.* **2004**, *301*, 197.
(50) Mo, Y.; Suzuki, T. *J. Chem. Phys.* **1998**, *109*, 4691.
(51) Martin, J. D. D.; Hepburn, J. W. *J. Chem. Phys.* **1998**, *109*, 8139.
(52) Blanksby, S. J.; Ellison, G. B. *Acc. Chem. Res.* **2003**, *36*, 255.
(53) Spirko, V.; Bunker, P. R. *J. Mol. Spectrosc.* **1982**, *95*, 381.
(54) Frey, J. G.; Felder, P. *Mol. Phys.* **1992**, *75*, 1419.
(55) Yang, S.; Bersohn, R. *J. Chem. Phys.* **1974**, *61*, 4400.
(56) Matsumi, Y.; Tonokura, K.; Kawasaki, M.; Inoue, G.; Satyapal, S.; Bersohn, R. *J. Chem. Phys.* **1991**, *94*, 2669.
(57) Lambert, H. M.; Dagdigian, P. J.; Alexander, M. H. *J. Chem. Phys.* **1998**, *108*, 4460.
(58) Regan, P. M.; Langford, S. R.; Orr-Ewing, A. J.; Ashfold, M. N. R. *J. Chem. Phys.* **1999**, *110*, 281.
(59) Langford, S. R.; Regan, P. M.; Orr-Ewing, A. J.; Ashfold, M. N. R. *Chem. Phys.* **1998**, *231*, 245.
(60) Manzhos, S.; Loock, H.-P.; Bakker, B. L. G.; Parker, D. H. *J. Chem. Phys.* **2002**, *117*, 9347.
(61) Rakitzis, T. P.; Samartzis, P. C.; Toomes, R. L.; Tsigaridas, L.; Coriou, M.; Chestakov, D.; Eppink, A. T. J. B.; Parker, D. H.; Kitsopoulos, T. N. *Chem. Phys. Lett.* **2002**, *364*, 115.
(62) Townsend, D.; Suits, A. G. Unpublished results.
(63) Kupriayanov, D. V.; Vasyutinskii, O. S. *Chem. Phys.* **1993**, *171*, 25.